Neuron, Vol. 20, 341–351, February, 1998, Copyright ©1998 by Cell Press

Known Calcium Channel α_1 Subunits Can Form Low Threshold Small Conductance Channels with Similarities to Native T-Type Channels

Alon Meir and Annette C. Dolphin*
Department of Pharmacology
University College London
London WC16BT
United Kingdom

Summary

Native T-type voltage-dependent calcium channels are low voltage–activated and have a small single channel conductance of 5–8 pS, which distinguishes them from any known cloned calcium channels whose conductances are 12–25 pS. Here, we show that when α_{1B}, α_{1E}, or α_{1C} are expressed in COS7 cells, which contain no endogenous calcium channel subunits or calcium channels, they each exhibit a 4–7 pS channel as well as a large conductance channel. At low depolarizations, or when the α_1 subunit is expressed in the absence of auxiliary α_2-δ or β subunits, the small conductance channels are seen alone, and their biophysical properties, including voltage dependence and kinetics of activation and inactivation, are very similar to native T-type calcium channels.

Introduction

Voltage-dependent calcium channels (VDCCs) in neurons and other cells have been divided into high and low voltage–activated (HVA and LVA or T-type) classes (Carbone and Lux, 1984; Bean, 1985; Nilius et al., 1985). Although a number of VDCCs have been cloned and identified with their native counterparts, the molecular nature of T-type VDCCs has so far eluded investigation (reviewed by Ertel and Ertel, 1997). However, their importance in the physiological and pathophysiological functioning of excitable cells makes this a problem of particular interest (Huguenard, 1996; Ertel and Ertel, 1997). Known cloned VDCCs consist of a pore-forming α_1 subunit, of which six subtypes have been identified at the molecular level (A, B, C, D, E, and S), and an auxiliary transmembrane α_2-δ and intracellular β subunit (reviewed by Tsien et al., 1995). T-type VDCCs have a small single channel conductance of 5–8 pS, usually measured in 90–110 mM Ba^{2+} (Carbone and Lux, 1987a; Fox et al., 1987a), which distinguishes them from any of the known cloned VDCCs, whose reported conductances range from 12–25 pS (Schneider et al., 1994; Wakamori et al., 1994; Bourinet et al., 1996). T-type VDCCs characteristically begin to activate at about −70 mV under physiological conditions, producing a maximum current at between −40 and −20 mV (Carbone and Lux, 1987b; Fox et al., 1987b; Huguenard, 1996). The current waveform is transient (Carbone and Lux, 1987b; Fox et al., 1987b) with a division into rapidly and more slowly inactivating subtypes (Chen and Hess, 1990; Huguenard and Prince, 1992; Tarasenko et al., 1997).

The α_{1E} clone has been put forward as a possible candidate for T-type current because it possesses some of the salient features, including low activation voltage, rapid inactivation, and similar or greater whole-cell current amplitude in Ca^{2+} compared to Ba^{2+} (Soong et al., 1993). Nevertheless, major discrepancies exist, the main one being that the single channel conductance reported for α_{1E} channels is 12–14 pS (Schneider et al., 1994; Wakamori et al., 1994). Furthermore, although activation and steady-state inactivation of expressed α_{1E} current occur at lower voltages than for some other cloned VDCCs (Soong et al., 1993; Stephens et al., 1997), their thresholds are not as low as for native T-type current.

We have expressed α_{1B}, α_{1C}, and α_{1E} VDCCs in COS7 cells, which contain no endogenous mRNA or protein for VDCC α_1 or accessory subunits or endogenous calcium channel currents (Berrow et al., 1997; Brice et al., 1997; Stephens et al., 1997). This system is therefore advantageous for the present study compared to several other expression systems, including *Xenopus* oocytes, which possess endogenous β and α_2-δ subunits and endogenous calcium currents (Singer-Lahat et al., 1992; Tareilus et al., 1997), or HEK293 cells, which also have endogenous calcium currents (Berjukow et al., 1996). For all three α_1 subunits, in addition to large conductance channels we have also observed low threshold small conductance single calcium channels, which have properties very similar to the native T-type channels that we have examined for comparison in undifferentiated NG108–15 cells.

Results

α_1 Subunits Can Form Small As Well As Large Conductance Channels

The calcium channel α_1 subunits α_{1B}, α_{1E}, or α_{1C} were transiently coexpressed in COS7 cells with α_2-δ and β_{2a} or β_3 subunits, and single calcium channel activity was recorded in the cell-attached mode. From a holding potential of −90 or −115 mV, at low depolarizations we observed small conductance calcium channels with amplitudes at −25 mV in 100 mM Ba^{2+} of -0.43 ± 0.05 pA for α_{1B}/α_2-δ/β_{2a} ($n = 5$; Figure 1a), -0.29 ± 0.02 pA for α_{1E}/α_2-δ/β_{2a} ($n = 5$; Figure 1b), and -0.25 ± 0.03 pA for α_{1C}/α_2-δ/β_{2a} ($n = 5$; Figure 1c). The single channel slope conductance of the small channels was similar for all α_1 subunits in this combination, being between 5 and 7 pS (Figure 1d). In each case, a larger conductance channel was also observed, particularly at more depolarized potentials (Figures 1a, 1b, and 1c), with characteristics very similar to those previously reported for α_{1B}, α_{1E}, and α_{1C} subunits in other systems (Schneider et al., 1994; Wakamori et al., 1994; Bourinet et al., 1996). The corresponding amplitudes were -1.18 ± 0.02 pA ($n = 5$), -0.62 ± 0.03 pA ($n = 5$), and -1.46 ± 0.02 pA ($n = 3$), respectively. For α_{1B}/α_2-δ/β_{2a} in 100 mM Ba^{2+}, the small conductance channels were first observed at −45 mV,

*To whom correspondence should be addressed.

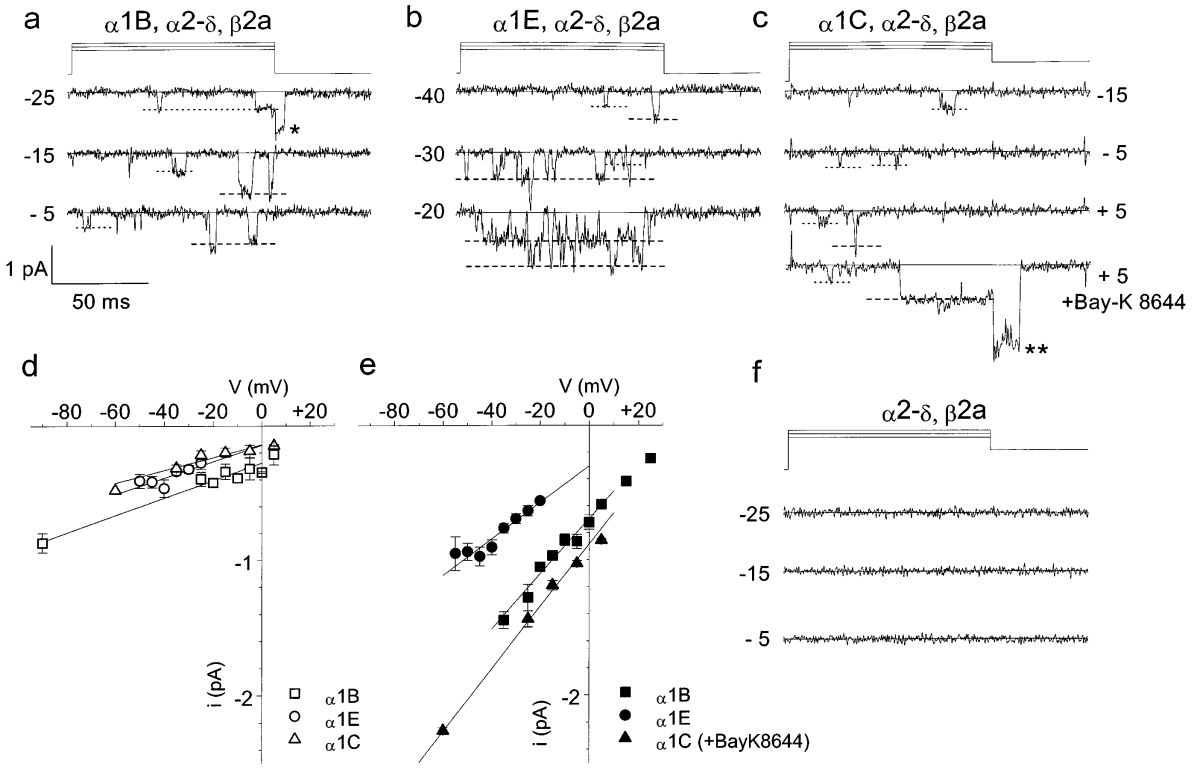

Figure 1. Expression of α_{1B}, α_{1E}, or α_{1C} VDCC in COS7 Cells Yields Both Small and Large Conductance Channels

(a–c) Calcium channels were recorded from cells transfected with α_{1B} (a), α_{1E} (b), and α_{1C} cDNA (c) together with α_2-δ and β_{2a}. Both small and large channels are observed in these patches. The solid horizontal lines on the current traces indicate the zero current level, the dotted lines indicate examples of the amplitude of the small channels, and the broken lines indicate the amplitude of the large channels. At the top of each column, the voltage protocol is indicated; for (a) and (b), the holding potential is −90 mV, both before and after the test pulse, and the voltage steps are indicated to the left of the traces. For (c), the holding potential is −115 mV before the pulse and −60 mV after it ends, and the voltage steps are indicated to the right of the current traces. The first three traces in (c) were recorded in the absence of S(−)-BayK8644. BayK8644 (10 μM) was then added to the bath, under conditions of dimmed lighting, and the lowest trace is an example at 5 mV in its presence. The asterisks indicate a prolonged tail current attributable to the large α_{1C} channel. All traces are leak subtracted.

(d) I–V relationships for the small channel expressed by the three α_1 subunits: α_{1B} (open squares), 5.5 ± 0.4 pS (n = 5); α_{1E} (open circles), 6.2 ± 1.4 pS (n = 5); and α_{1C} (including experiments both in the presence and absence of BayK8644; open triangles), 5.2 ± 0.8 pS (n = 5).

(e) I–V relationships for the large conductance channels expressed by all three α_1 subunits: α_{1B} (closed squares), 19.7 ± 2.8 pS (n = 5); α_{1E} (closed circles), 14.8 ± 1.9 pS (n = 5); and α_{1C} (with BayK8644; closed triangles), 22.7 ± 0.8 pS (n = 3). The fits in (d) and (e) only included data below 0 mV (d) or 5 mV (e), to avoid the nonlinear region of the relationship at more positive potentials.

(f) Representative leak-subtracted episodes at the indicated voltages (left) with no activity, obtained from cells transfected with α_2-δ and β_{2a} without any α_1 subunit (representing 15 patches).

whereas the large conductance channels were first observed at −35 mV (Table 1), and the small and large channels had single channel conductances of 5.5 ± 0.4 and 19.7 ± 2.8 pS, respectively (n = 5; Figures 1d and 1e). For α_{1E}, the two conductance levels were 6.2 ± 1.4 and 14.8 ± 1.9 pS (n = 5; Figures 1d and 1e). Both small and large conductance α_{1E} channels were seen at significantly lower depolarizations than for α_{1B} (Table 1). However, at higher depolarizations, the small conductance channel was often difficult to distinguish because all of the α_{1E} patches contained multiple channels (e.g., Figure 1b, step to −20 mV).

For expression of α_{1C}/α_2-δ/β_{2a}, similar results were obtained. Figure 1c illustrates an experiment in which 10 μM of the L-type calcium channel agonist S(−)-BayK8644 was applied during the recording. The small conductance channels were observed both in the absence of BayK8644 and in its presence (Figure 1c). In this experiment, brief openings of the large conductance channels were observed in the absence of BayK8644. These openings were prolonged as expected in its presence, and long tail currents were observed (Figure 1c [**]), whereas the openings of the small conductance channel were not affected (Figure 1c, lowest trace). The small α_{1C} channels were first observed at −45 mV and the large α_{1C} channels at −25 mV (Table 1). In the absence of BayK8644, the large conductance α_{1C} channel was not observed in every patch containing a small conductance channel. From 23 patches, 6 of 12 patches with channel activity apparently contained only a small conductance channel (see also Figure 5c). However, in the presence of BayK8644, the large channel was observed in every patch that contained a small conductance channel (4 of 6 total patches). Thus, in the absence of the L-type

Table 1. Distribution of Voltages at which Small and Large Conductance Channels Were First Observed

Voltage Step	α_{1E}	α_{1E}	α_{1B}	α_{1B}	α_{1C}	α_{1C}
mV	small	large	small	large	small	large
−65	−	−	−	−	−	−
−55	5 (29%)	4 (25%)	−	−	−	−
−45	8 (47%)	9 (56%)	1 (5%)	−	1 (9%)	−
−35	4 (24%)	2 (13%)	7 (35%)	4 (24%)	7 (64%)	−
−25	−	1 (6%)	10 (50%)	7 (41%)	2 (18%)	1 (17%)
−15	−	−	2 (10%)	6 (35%)	1 (9%)	3 (50%)
−5	−	−	−	−	−	2 (33%)
Number of Experiments	17	16	20	17	11	6
Statistical significance	$p < 0.01$ versus α_{1B} and α_{1C} small	NS versus α_{1E} small		$p < 0.01$ versus α_{1B} small		$p < 0.001$ versus α_{1C} small

Recordings were made from cell-attached patches from cells transfected with α_{1E}, α_{1B}, or α_{1C} together with α_2-δ and β_{2a}, using 100 mM Ba^{2+}. For each experiment, the depolarization at which the small and large conductance channels were first observed was determined as the voltage at which at least 5 openings were present in 20-50 100 ms episodes of a single experiment. The significance of the differences between the distributions was determined by χ^2 test. NS, not significant.

channel agonist, it is possible that the openings of the large conductance channels were too short to be observed. The conductances of the small and large α_{1C} channels were 5.2 ± 0.8 pS (n = 5) and 22.7 ± 0.8 pS (n = 3), respectively, in 100 mM Ba^{2+} (Figures 1d and 1e).

The small conductance calcium channel is not endogenous to COS7 cells; as in all experiments in which α_{1B} and α_{1E} were expressed with accessory subunits, the small conductance channel was only observed in patches that also contained a large conductance channel (39 of 151 total patches for α_{1B}/α_2-δ/β_{2a} or β_3 and 19 of 38 for α_{1E}/α_2-δ/β_{2a}). Furthermore, no inward currents were observed in cells transfected with only α_2-δ/β_{2a} (Figure 1f; n = 15 patches) or in cells transfected with green fluorescent protein (GFP) alone (13 patches). This agrees with the lack of whole-cell Ba^{2+} currents in COS7 cells transfected with GFP alone (Berrow et al., 1997; Brice et al., 1997; Stephens et al., 1997).

For α_{1B}, the properties of the small channels were analyzed in more detail because patches without multiple channel openings were more often obtained than for α_{1E} (see Figure 1b, −20 mV trace), and therefore the openings of the small and large conductance channels could be distinguished more easily. The small α_{1B} channel openings tended to cluster at the beginning of sweeps, particularly at higher depolarizations. This separation was particularly noticeable in some patches from α_{1B}/α_2-δ/β_{2a} transfected cells, where a clear temporal difference between the openings of the small and large conductance channels was seen (Figure 2a; 10 mM Ba^{2+}). The ensemble-averaged current at −25 mV (Figure 2b) shows the rapidly activating and inactivating nature of the small conductance channels. The small channels consistently showed more rapid activation (in terms of latency to first opening) than the large channels, particularly at low depolarizations, and the first latency had a strong voltage dependence (Figure 2c). Furthermore, the all-points histogram profiles (Figure 2d) demonstrate the dominance of the small channels at low depolarizations and the activation of the large channels at greater depolarizations. The possibility of a subconductance state for the small α_{1B} channel is suggested by the asymmetric peak at −35 mV, but this has not been analyzed further here.

Evidence for similar divalent cation permeability of the small and large conductance channels was obtained by comparing their conductance in two different Ba^{2+} concentrations. The conductance of the large α_{1B} channel was reduced by 14.2% from 19.7 pS in 100 mM Ba^{2+} to 16.9 ± 2.7 pS (n = 4; Figure 2e) in 10 mM Ba^{2+}, whereas the small channel conductance was reduced by 29.1%, from 5.5 pS to 3.9 ± 0.8 pS (n = 4; Figure 2e). Preliminary data (not shown) also indicate that the small α_{1B} channels exhibit similar amplitudes at 5 mV in 100 mM Ba^{2+} (−0.21 pA, n = 2) and 100 mM Ca^{2+} (−0.17 ± 0.03 pA, n = 3). For the small α_{1E} channels, the amplitudes of the elementary currents measured at −15 mV were identical in 100 mM Ba^{2+} and 100 mM Ca^{2+}, being −0.23 pA (n = 2) and −0.23 ± 0.03 pA (n = 3), respectively.

In contrast to the data for β_{2a}, no clear temporal separation between the small and large conductance channels was seen for the α_{1B}/α_2-δ/β_3 combination, where the large conductance channel openings were also clustered near the start of sweeps (n = 9; data not shown). This is in agreement with the opposite effects of these two β subunits on macroscopic calcium channel currents, β_{2a} slowing and β_3 enhancing the kinetics of inactivation of currents resulting from expressed α_1 subunits (Olcese et al., 1994; De Waard and Campbell, 1995).

Properties of the Small Conductance Channels When α_{1B} Subunits Are Expressed Alone

In cells transfected with α_{1B} in the absence of α_2-δ or β subunits, the small channel was observed in 14 of 42 cell-attached patches. In 5 of 14 of the patches containing channel activity, the small channel was seen in the absence of the large conductance channel (Figures 3a–3e; 100 mM Ba^{2+}), and its properties could be examined in isolation. The small channels usually inactivated during a 100 ms pulse, particularly at higher depolarizations (Figure 3a), as also seen in the ensemble-averaged current at 5 mV (Figure 3b). The time constant of inactivation (τ_{inact}) was 39.2 ± 8.0 ms at this potential (n = 3;

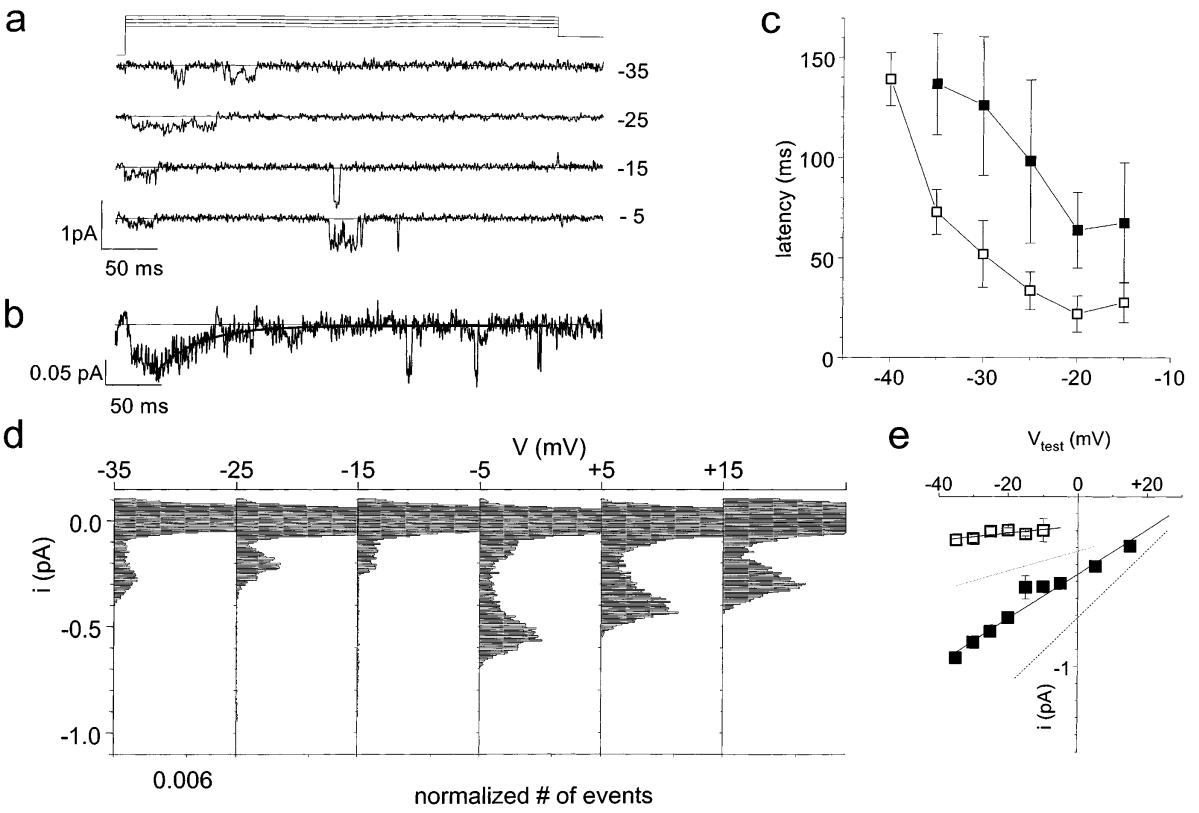

Figure 2. The Small Conductance α_{1B} Channel Is Lower Voltage Activated Than the Large Conductance Channel and Is Similarly Ba^{2+} Permeable

Recordings were performed from cells transfected with the α_{1B}/α_2-δ/β_{2a} combination.

(a) Individual current responses to different depolarization steps from a holding potential of −115 mV with 10 mM Ba^{2+} in the patch pipette. The small channel opens at the beginning of the voltage step and inactivates during the 400 ms pulse. Both short (−35 mV trace) and longer openings (−25 mV trace) are seen in this patch. At higher depolarizations, the larger channel is activated (traces to −15 and −5 mV).

(b) An ensemble-averaged current response for the 400 ms step to −25 mV (an average of 10 single episodes). The ensemble current inactivates with an exponential decay (solid line), with τ_{inact} equal to 39.0 ms; the late inward deflections are single events of the large α_{1B} channel.

(c) Latency to first opening as a function of the test voltage, measured separately for the small (open squares) and large (closed squares) α_{1B}/α_2-δ/β_{2a} channels in 10 mM Ba^{2+} (mean ± SEM; n = 6). The latency was determined as the mean time to first opening for both current levels.

(d) All-point histograms from the same experiment shown in (a). These were constructed from 10 episodes of 400 ms duration at each voltage, filtered at 500 Hz. The bin width was 6.25×10^{-3} pA. The closed level peak was truncated to better visualize the open level peak of the small conductance channel.

(e) An I–V plot of the small and large channels with 10 mM Ba^{2+} as the charge carrier. The small (open squares) and large (closed squares) single channel conductances are 3.9 ± 0.8 pS (n = 4) and 16.9 ± 2.7 pS (n = 4), respectively. The dotted and broken lines represent the data for the respective α_{1B} channels in 100 mM Ba^{2+}, from Figures 1d and 1e.

Figure 3b). The single channel conductance of the small α_{1B} channels in patches where they were observed in isolation was 4.2 ± 0.3 pS, and the amplitude at −25 mV was −0.27 ± 0.02 pA (n = 5; Figure 3c). Steady-state inactivation is demonstrated in Figure 3d, where the small channel was completely inactivated when the holding potential was depolarized to −55 mV. Although many of the openings of the small conductance α_{1B} channel were brief, long openings were also observed (e.g., Figures 2a and 3a). The long openings gave rise to a slowly deactivating tail current (Figures 3a [*] and 3e). In ensemble-averaged currents, the tail current decayed with a time constant (τ_{deact}) of 12.8 ± 5.1 ms at −60 mV (n = 3; Figure 3e). Slowly deactivating tail currents associated with the small channels were also seen in patches containing both large and small channels (e.g., Figure 1a [*]).

Comparison of Native T-Type Channels with Small Conductance Channels Resulting from Expressed α_1 Subunits

To determine whether the properties of the small conductance single channels observed here are similar to endogenous T-type calcium channels, we examined, under the same conditions, T-type single channel currents in undifferentiated NG108–15 cells (a hybridoma cell line of a mouse neuroblastoma and a rat glioma). The single T-type channels in cell-attached patches were of similar amplitude (−0.21 ± 0.02 pA at −25 mV in 100 mM Ba^{2+}, n = 3) to the small α_{1B}, α_{1E}, and α_{1C} channels observed here (Figure 4a). A preliminary comparison of permeability at 5 mV in 100 mM Ba^{2+} and 100 mM Ca^{2+} gave identical elementary current amplitudes (−0.19 ± 0.02 pA [n = 3] and −0.19 pA [n = 2], respectively; data not shown). From the ensemble-averaged currents at 5

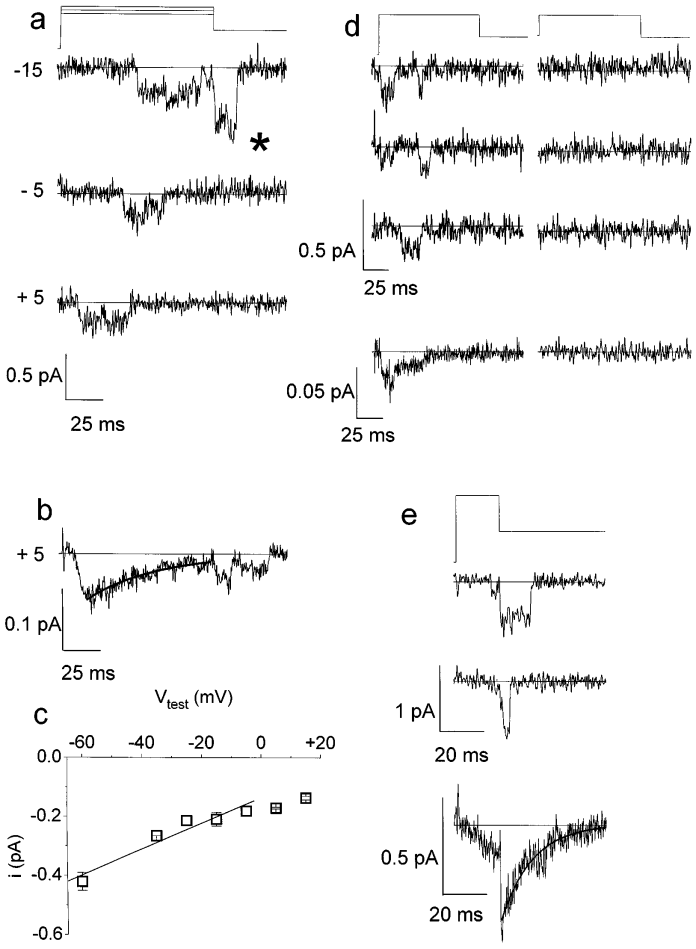

Figure 3. Properties of the Small Conductance α_{1B} Channels When α_{1B} Is Expressed Alone

Cell-attached patches were recorded with 100 mM Ba^{2+} from cells transfected with α_{1B} alone.

(a) Individual current responses to the depolarization steps shown (−15 to 5 mV) from a holding potential of −115 mV in a patch containing only the small conductance channel; the asterisk indicates tail current.

(b) Ensemble-averaged current of 39 episodes in response to a voltage step to 5 mV as in (a). The current inactivates following a single exponential decay (solid curve) with a τ_{inact} of 42.7 ms.

(c) I–V relationship for the small channel when expressed alone (conductance, 4.2 ± 0.3 pS; n = 5). The fit only included data below 0 mV, to avoid the nonlinear region of the relationship at more positive potentials.

(d) Steady-state inactivation of the small α_{1B} channel. In the left column, the holding potential is −115 mV, and the three upper single responses are examples of the activity of the small channel at a test potential of −5 mV. In the right column are three examples of responses of the same patch to the same test potential, 30 s after the holding potential was changed to −55 mV . The lowest traces in both columns are the ensemble averages of 30 episodes in each condition.

(e) Tail currents at −60 mV of the small conductance channel. The prepulse holding potential was −115 mV; the activating pulse of 20 ms was to 15 mV. The two upper traces are single responses, showing that the channel remains open after the repolarization (see also Figure 1a and upper trace of [a] in this Figure). The lowest trace is an ensemble of 30 such responses from the same patch. The tail current deactivation was best fitted with one exponent (solid curve), with a time constant (τ_{deact}) of 14.3 ms.

mV, the native T-type channels showed slightly faster inactivation kinetics than the small conductance α_{1B} channels (Figure 4b; τ_{inact} = 21.7 ± 2.5 ms, n = 3). The single channel conductance was also similar to that of the small conductance α_1 channels (4.5 ± 0.8 pS, n = 3; Figure 4c), and as expected the T-type channels also showed complete steady-state inactivation at −55 mV (Figure 4d). The tail current deactivation of the T-type channels studied here was similar to the small conductance α_{1B} channels (Figure 4e; τ_{deact} = 8.3 ± 1.5 ms at −60 mV, n = 8).

In COS7 cells transfected with α_{1E} alone, large as well as small conductance channels were almost always observed (in 11 of 49 total patches), and it was therefore difficult to compare their properties to those of native T-type channels. However, in one patch the small α_{1E} channel was observed alone (Figure 5a). The ensemble-averaged current at −15 mV decayed with a τ_{inact} of 15.1 ms (Figure 5b). The slope conductance of this channel was 5.2 pS. It was also possible to examine the properties of the small conductance α_{1C} channel in isolation in patches from cells transfected with α_{1C}/α_2-δ/β_{2a}, recorded in the absence of BayK8644, where in 6 of 12 patches with channel activity no large conductance channels were observed (Figure 5c). The ensemble-averaged current at −15 mV inactivated with a τ_{inact} of 38.0 ms (Figure 5d). At 5 mV, the current inactivated more rapidly, and τ_{inact} was 17.7 ± 9.7 ms (n = 3).

Another important similarity with native T-type channels is that the small conductance channels survive in excised inside-out patches. When a patch containing both small and large conductance α_{1C} channels, in the presence of BayK8644, was excised into the bath solution (Figure 5e [left]), the large conductance α_{1C} channel was rapidly lost, whereas the small channel was retained (Figure 5e [right]).

Discussion

In several previous studies, we have not found COS7 cells to contain endogenous calcium channel subunit mRNA or protein, from evidence obtained by RT-PCR, immunocytochemistry, and whole-cell electrophysiological recording (Berrow et al., 1997; Brice et al., 1997; Stephens et al., 1997). This, together with the lack of

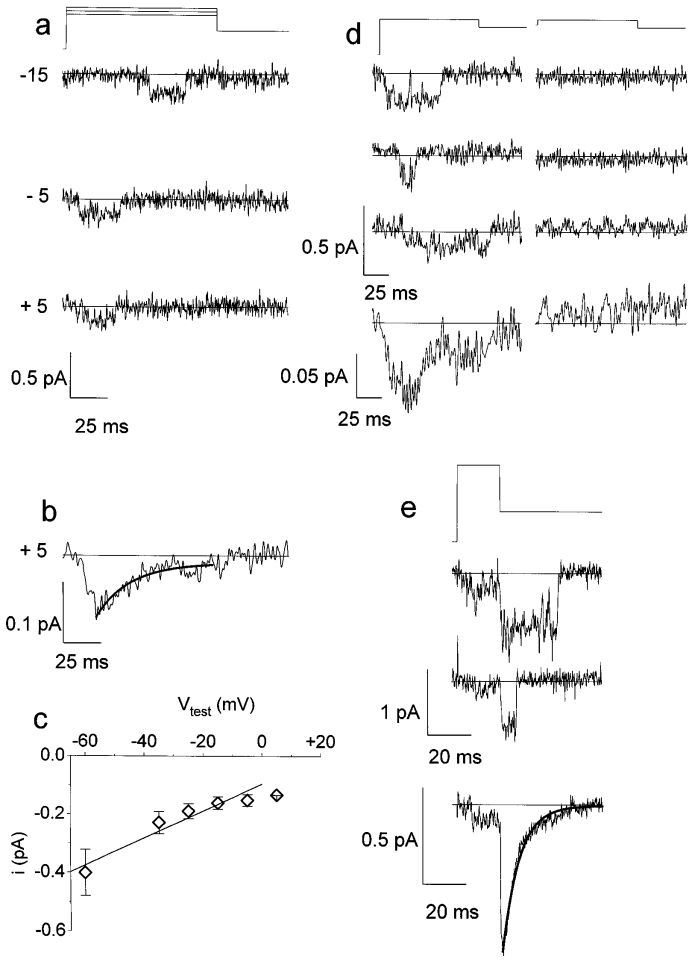

Figure 4. Native T-Type Channels in Undifferentiated NG108–15 Cells Possess Properties Similar to the Expressed α_1 Small Channels

(a) Individual current responses to the depolarization steps stated at the left of each trace (−15 to 5 mV) from a holding potential of −115 mV in a patch containing T-type channels (100 mM Ba^{2+}).

(b) Ensemble-averaged current of 44 episodes in response to a voltage step to 5 mV. Inactivation follows a single exponential decay (solid curve) with a τ_{inact} of 22.3 ms.

(c) I–V relationship for T-type channels (conductance, 4.5 ± 0.8 pS; n = 3). The fit only included data below 0 mV, to avoid the nonlinear region of the relationship at more positive potentials.

(d) Steady-state inactivation of T-type single channel currents. In the left column, the holding potential is −115 mV, and the three upper single responses are examples of the activity of the channel at a test potential of −45 mV. In the right column are three examples of responses of the same patch to the same test potential, 30 s after the holding potential was changed to −55 mV. The lowest traces in both columns are the ensemble-averaged currents for 25 episodes in each condition.

(e) Tail currents for T-type channels at −60 mV. The prepulse holding potential was −115 mV, the activating pulse of 25 ms was to 25 mV. The two upper traces are single responses, showing that the channel remains open after the repolarization. The lowest trace is an ensemble of 70 such responses from the same patch. The deactivation was best fitted with one exponent (solid curve), with a time constant (τ_{deact}) of 7.5 ms.

any single calcium channel activity recorded from cell-attached patches in COS7 cells in the absence of transfected α_1 subunits, provides strong evidence that the small conductance channels observed here are not endogenous to this cell type. The present results are consistent with the hypothesis that small conductance LVA channels may be formed by α_{1B}, α_{1E}, and α_{1C} VDCCs, which can exist in a small conductance mode. This is supported by the finding that small conductance channels are observed in every patch in which a large conductance channel is present, and that the different α_1 subunits produce small channels with significantly different voltage-dependent properties (Table 1). These observations also provide evidence that the behaviors of the small and large conductance channels are not independent of each other, unlike the behaviors expected if the small channels described here were endogenous T-type channels indirectly induced by the heterologous expression of the calcium channel α_1 subunits. The small channels were not observed in patches from which the large channels were absent, except in some patches in which α_{1C} channels were recorded in the absence of BayK8644, when openings of the large α_{1C} channels may have been too short to be observed, and in some patches from cells transfected with α_{1B} or α_{1E} in the absence of accessory subunits.

The small conductance LVA channels formed by α_{1B}, α_{1E}, and α_{1C} have properties very similar to those of native T-type channels in other systems. These similarities include: (1) the small single channel conductance in 100 mM Ba^{2+} (Carbone and Lux, 1987a; Fox et al., 1987a); (2) low voltage of activation (Carbone and Lux, 1987a; Fox et al., 1987a); (3) complete steady-state inactivation at a depolarized holding potential such as −55 mV (Carbone and Lux, 1987a; Fox et al., 1987a); (4) rapid inactivation during voltage steps (Carbone and Lux, 1987a); (5) strongly voltage-dependent first latency (Droogmans and Nilius, 1989); (6) single channel activity that is retained in excised patches (Carbone and Lux, 1987a); (7) a slow component of tail current deactivation (Armstrong and Matteson, 1985); (8) the presence of both brief and prolonged openings (Carbone and Lux, 1987a; Fox et al., 1987a); (9) a high probability of observing episodes with no channel activity (see data in the Figure 6 legend) (Droogmans and Nilius, 1989); and (10) similar current amplitude with Ba^{2+} and Ca^{2+} as charge carriers.

By RT-PCR, using primers that recognize both rat and mouse sequences, we have found undifferentiated NG108–15 cells to contain transcripts for α_{1A}, α_{1B}, α_{1C}, and α_{1E}, as well as for α_2-δ and β_1–β_4 (C. N. Wyatt, K. M. Page, N. L. Brice, N. S. Berrow, and A. C. D., unpublished data), and the NG108–15 T-type channels could possibly be formed from any or all of these α_1 subunits. If, as suggested by the present findings, more than one type

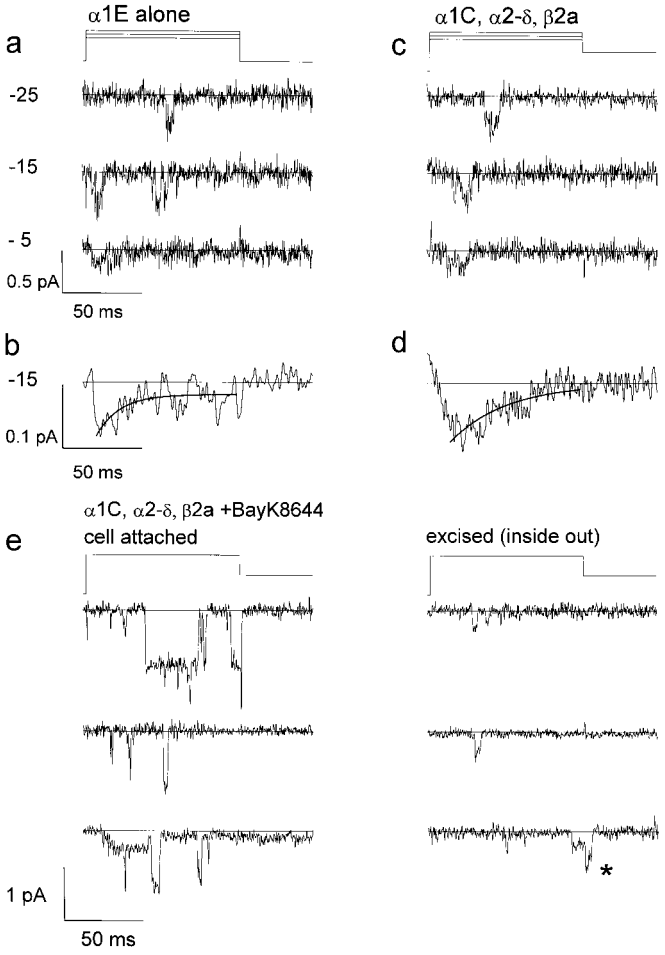

Figure 5. T-Type Properties of the Small α_{1E} and α_{1C} Channels

(a) A patch recorded from a cell transfected with α_{1E} alone, which possessed only the small channel, showing individual leak-subtracted current responses to different depolarization steps from a holding potential of −115 mV (100 mM Ba^{2+}). The test potential (−25 to −5 mV) is indicated on the left.

(b) An ensemble-averaged current of 20 episodes in response to a voltage step to −15 mV from the same patch as (a). It inactivates incompletely following a single exponential decay (solid curve) with a τ_{inact} of 15.1 ms.

(c) A patch from a cell transfected with α_{1C}/α_2-δ/β_{2a}, in which only the small channel was observed, showing individual leak-subtracted current responses to the same depolarization steps shown in (a) from a holding potential of −115 mV (100 mM Ba^{2+}).

(d) An ensemble average (20 episodes) of α_{1C} currents at −15 mV from the same patch as in (c). It inactivates following a single exponential decay (solid curve) with a time constant of 38.0 ms.

(e) On the left are three traces showing the presence of both a large and a small channel, from a cell-attached patch from an α_{1C}/α_2-δ/β_{2a} transfected cell (holding potential, −115 mV; test potential, −5 mV) in 10 μM BayK8644; on the right are three traces at the same potential following excision to form an inside-out patch (the asterisk indicates tail current of small channel).

of α_1 subunit may be involved in the expression of native T-type calcium channels, this would offer an explanation for the range of activation voltages and inactivation kinetics of these currents observed in different cell types (Akaike et al., 1989; Chen and Hess, 1990; Huguenard and Prince, 1992; Kobrinsky et al., 1994; Tarasenko et al., 1997). It would also explain the diverse and inconsistent pharmacology of T-type channels, with sensitivity to 1,4-dihydropyridine antagonists but not agonists (Akaike et al., 1989; Tarasenko et al., 1997), similar to α_{1E} (Stephens et al., 1997), and rapidly reversible block by ω-conotoxin GVIA (McCleskey et al., 1987; Kobrinsky et al., 1994) and ω-agatoxin IVA (Kobrinsky et al., 1994) having been observed in some cell types but not others. It is of relevance here that expression in HEK293 cells of α_{1B} in the absence of accessory subunits produced a rapidly inactivating whole-cell current that was blocked reversibly by ω-conotoxin GVIA (Williams et al., 1992). Furthermore, similar permeability to Ca^{2+} and Ba^{2+} (a hallmark of α_{1E} channels) is often observed for T-type current, but in thalamic reticular neurons the T-type currents are more permeable to Ba^{2+} than Ca^{2+} (Huguenard and Prince, 1992). Our preliminary finding is that the small α_{1E} channels show the same amplitude in Ca^{2+} as in Ba^{2+}, whereas the small α_{1B} channels show a slightly lower amplitude in Ca^{2+}. It is possible that the small conductance α_1 subunits will show similar pharmacology to the cognate large conductance channels, but this is not necessarily the case, as accessory subunits—particularly α_2-δ—have a marked effect on the pharmacology of expressed calcium currents (Brust et al., 1993; Gurnett et al., 1997). A pharmacological examination of the properties of the small conductance calcium channels formed from expressed α_1 subunits is currently in progress.

The molecular composition of these small conductance α_1 subunit channels cannot be unequivocally identified from the present results. The predominance of small conductance channels obtained with α_{1B} (and, in one instance, α_{1E}) in the absence of expressed α_2-δ and β subunits suggests that the small conductance mode is favored when the α_1 subunit is not under the influence of one or both of these accessory subunits. However, it is clear from the present results that α_1 subunits, expressed alone, may form large as well as small conductance channels; and conversely, small conductance channels are still observed in the presence of the accessory subunits. Although it has been shown that there is a reversible association between α_1 and accessory α_2-δ subunits (Liu et al., 1995), it is not clear whether this occurs under physiological conditions. Similarly, although the interaction between α_1 and β subunits is of

high affinity in vitro (De Waard et al., 1995), the association may be voltage-dependent and favored at depolarized potentials (see Dolphin, 1996, for a discussion of this point). Thus, it is possible that native T-type currents may consist of α_1 subunits not associated with either an α_2-δ subunit, a β subunit, or both. There is some evidence from an antisense study for the lack of association of T-type currents with a β subunit (Lambert et al., 1997). In agreement with this, β_{2a} had no apparent effect on the small conductance channels, since the inactivation rate of the small channels was similarly rapid in the presence of β_{2a} or in the absence of a β subunit (compare Figures 2b and 3b). However, the lack of involvement of either α_2-δ or β in the formation of the small α_1 channels will require further experimentation with specific combinations of subunits and more detailed analysis.

Several α_1 subunits exhibit activation in the range of -40 to -20 mV in physiological divalent cations (Soong et al., 1993; De Waard and Campbell, 1995), and their activation often shows two components of voltage dependence (Olcese et al., 1996). It has been suggested that, of the known cloned calcium channels, α_{1E} is the best candidate for the molecular counterpart of LVA calcium channels (Soong et al., 1993), and we have found that α_{1E} expressed in COS7 cells in the absence of accessory subunits forms a whole-cell current with some similarities to T-type current (Stephens et al., 1997). Our present results would agree with this, as the small conductance α_{1E} channels were first observed at -55 mV in 100 mM Ba^{2+} (which produces a shift due to charge screening of about 25 mV, compared to physiological saline [Elmslie, 1997]). Nevertheless, the small α_{1B} and α_{1C} channels were also first observed at hyperpolarized potentials (-45 mV in 100 mM Ba^{2+}). Furthermore, for both α_{1B} and α_{1C}, the small conductance channels were seen at significantly lower depolarizations than their respective large conductance channels (Table 1). Therefore, the small α_{1B} and α_{1C} channels also have the requisite biophysical properties to contribute to native T-type channels.

Since all of the α_1 subunits examined in the present study are able to form large as well as small conductance channels, it is likely that this is the reason no distinct low threshold component was observed previously in whole-cell current recordings in COS7 cells (Berrow et al., 1997; Brice et al., 1997; Page et al., 1997; Stephens et al., 1997). This point is also well illustrated from a comparison of ensemble averages of an α_{1B}/α_2-δ/β_{2a} patch in which multiple openings (including more than one small conductance channel) were present (Figures 6a and 6b), an α_{1B} small conductance channel alone (Figure 6c) and a native NG108–15 T-type channel (Figure 6d). The component of ensemble-averaged current in Figure 6a that results from the openings of the small conductance channels is only distinguishable in this case because of the high ratio of small to large channels apparent in the patch (Figure 6b). The activation phase of the current–voltage (I–V) relationship from data in Figure 6a can only be well fitted by a double Boltzmann relationship (Figure 6e, see legend). The LVA component activates in a similar range to the small conductance channels shown in Figures 6c and 6d. In most patches, the apparent proportion of small to large conductance channels is usually lower, and the ensemble-averaged I–V relationships do not have a pronounced LVA component, being similar to those observed in whole-cell experiments (Page et al., 1997; Stephens et al., 1997).

T-type calcium current is often observed in neurons and in other cell types early in development (Beam and Knudson, 1988; Barish, 1991) or in undifferentiated cells (Chen and Hess, 1990), and it is possible that particular VDCC α_1 subunits are selectively expressed under these conditions, before the appearance of accessory subunits. However, from our results, the absence of accessory subunits does not result exclusively in small conductance channels, and we can therefore put forward several possibilities for the composition of native T-type channels. It is feasible either that the α_1 subunits interact with an unknown associated protein that maintains the channels formed from these α_1 subunits in the LVA small conductance mode, or that there may be a lack of association with a subunit or associated protein whose presence normally promotes the expression of the large conductance mode. An alternative possibility is that channel oligomerization occurs, as previously suggested from experiments on reconstituted native calcium channels (Hymel et al., 1988). It is also feasible that there is post-translational modification of the α_1 subunit, but we have no direct evidence for this. In conclusion, the results described here suggest that VDCC α_1 subunits can form, as well as larger conductance channels, small channels with marked similarities to native T-type channels.

Experimental Procedures

Materials

The following cDNAs were used: rat α_{1E} (GenBank accession number L15453; Soong et al., 1993); rat brain α_{1C}-II (M67515; Tomlinson et al., 1993) from Dr. T. Snutch (University of British Columbia, Vancouver, Canada); rabbit α_{1B} (D14157; Fujita et al., 1993) from Dr. Y. Mori (Seiriken, Okazaki, Japan); rat β_{2a} (M80545; Perez-Reyes et al., 1992) and β_3 (M88751; Castellano et al., 1993) from Dr. E. Perez-Reyes (Loyola University, Chicago); and the full-length rat α_2-δ (neuronal splice variant, M86621; Kim et al., 1992) from Dr. H. Chin (National Institutes of Health, Bethesda, MD). The S65T mutant of green fluorescent protein (GFP) was provided by Dr. S. Moss (University College London), and the *mut-3* GFP mutant was provided by Dr. T. Hughes (Yale University, New Haven, CT). All cDNAs were subcloned, using standard techniques, into the *pMT2* expression vector (Genetics Institute, Cambridge, MA) for transient expression in COS7 cells. S(−)-BayK8644 was obtained from RBI (Natick, MA).

Transfection of COS7 Cells

COS7 cells were cultured and transfected by electroporation, essentially as described previously (Campbell et al., 1995). The α_1, α_2-δ, β, and either S65T or *mut-3* GFP cDNAs were used for transfection at 15 (or 20 when α_2-δ and β were absent), 10, 5, and 1 μg, respectively. When all subunits were not included, the total amount of plasmid used for transfection was retained at 31 μg by the addition of empty *pMT2* vector. Cells were maintained at 37°C and then replated using a nonenzymatic cell dissociation medium (Sigma) and kept at 25°C prior to electrophysiological recording. Successfully transfected cells were identified by expression of GFP. Maximum GFP fluorescence and Ca^{2+} channel expression were observed between 2 and 4 days posttransfection (Brice et al., 1997).

Electrophysiological Recording

All recordings were performed on GFP-positive cells at room temperature (20°C–23°C). Recording pipettes were pulled from borosilicate tubes (World Precision Instruments, Sarasota, FL), coated with Sylgard (Sylgard 184, Dow Corning, Wiesbaden, Germany), and fire

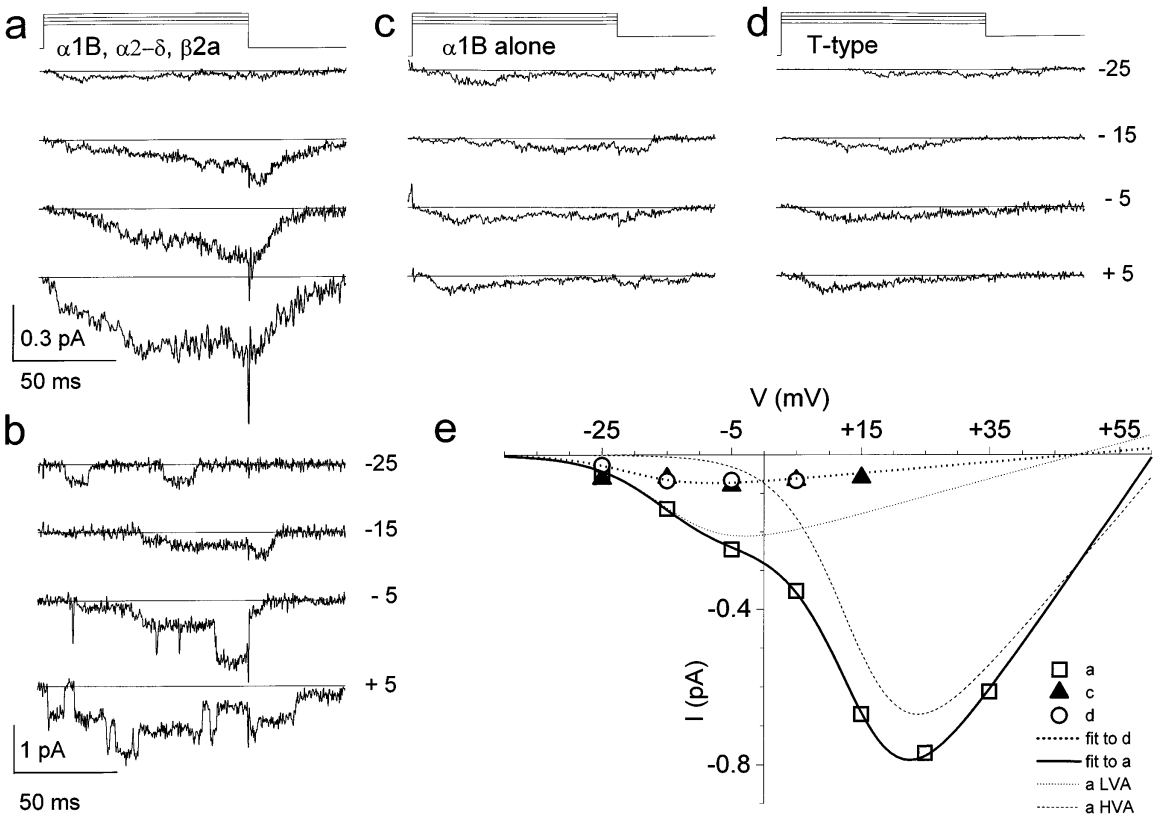

Figure 6. A Comparison of Ensemble-Averaged Currents from Patches Containing Both Large and Small α_{1B} Channels, the α_{1B} Small Channel Alone, or a Native T-Type Channel

(a) Ensemble-averaged currents (35 consecutive episodes each) at −25, −15, −5, and 5 mV for an experiment in which both small and large α_{1B} channels were recorded from a cell transfected with α_{1B}/α_2-δ/β_{2a} (100 mM Ba^{2+}). The number of blank episodes (containing no channel activity) at each potential were 25, 6, 7, and 4, respectively. The ensemble traces at −25 and −15 mV are constructed from openings of only the small channel, as it is below the threshold for the large channel. The slow tail currents are due to the slowly deactivating small channels (see −15 mV trace in [b]).

(b) Examples of single channel recordings from the same patch and at the same potentials as in (a). This patch is atypical in that it appeared to have an equivalent number of apparent small and large channels (three to four).

(c) Ensemble-averaged currents at −25 (25 consecutive episodes, including 13 blanks), −15 (29 episodes, 10 blanks), −5 (37 consecutive episodes, 11 blanks), and 5 mV (30 episodes, 7 blanks) for an experiment in which only a small α_{1B} channel was recorded from a cell transfected with α_{1B} alone (100 mM Ba^{2+}).

(d) Examples of ensemble-averaged currents at −25 (25 episodes, 19 blanks), −15 (30 episodes, 11 blanks), −5 (25 episodes, 7 blanks), and 5 mV (30 episodes, 8 blanks) for an experiment in which a native T-type channel was recorded from NG108–15 cells (100 mM Ba^{2+}).

(d) I–V relationship for the ensemble-averaged currents from the patch shown in (a); the peak current was measured for each trace. The I–V relationship (open squares) was fitted with a double Boltzmann function (solid line).

$I = [G_{max1}(V - V_{rev1})/(1 + \exp[(V_{h1} - V)/k_1])] + [G_{max2}(V - V_{rev2})/(1 + \exp[(V_{h2} - V)/k_2])]$, where G_{max} is maximum conductance, V_h is the voltage at which 50% of the current is activated, V_{rev} is the null potential, and k is the slope factor. The values for the parameters are: G_{max1}, 4.7 pS; G_{max2}, 19.8 pS; V_{rev1}, 48.7 mV; V_{rev2}, 63 mV; V_{h1}, −14.4 mV; V_{h2}, 14.2 mV; k_1, 5.4 mV; and k_2, 5.1 mV. V_{rev1} was constrained to the reversal potential obtained for a ramp I–V for the patch shown in (d), and V_{rev2} was constrained to the value obtained for a ramp I–V for the patch shown in (a). The two components 1 (LVA, dotted line) and 2 (HVA, broken line) of this function are also plotted individually using the parameters above. The I–V relationship for the NG108–15 T-type current (from [d]) is also plotted (open circles) and fitted with a single Boltzmann function (bold broken line). G_{max}, 1.42 pS; V_{rev}, 48.7 mV; V_h, −12.7 mV; and k, 8.5 mV. V_{rev} was constrained to the same value as V_{rev1} above. For comparison, the I–V relationship for the data from (c) for α_{1B} alone is also plotted (closed triangles).

polished to form high resistance pipettes (~10 MΩ with 100 mM $BaCl_2$). The composition of the bath solution, designed to zero the resting membrane potential and kept constant throughout this study, was (in mM): 135 K aspartate, 1 $MgCl_2$, 5 EGTA, and 10 HEPES (titrated with KOH [pH 7.3]) adjusted to an osmolarity of 320 mOsm with sucrose. The membrane potential in this external solution was -0.1 ± 0.9 mV ($n = 4$), recorded with 3M KCl-filled sharp microelectrodes. Patch pipettes were filled with a solution of three different compositions (in mM): 100 $BaCl_2$ or $CaCl_2$, 10 TEACl, 10 HEPES, and 200 nM TTX; or 10 $BaCl_2$, 130 TEACl, 10 HEPES, and 200 nM TTX. All pipette solutions were titrated with TEAOH to pH 7.4 and adjusted to an osmolarity of 320 mOsm with sucrose.

Seals were usually >20 GΩ. The data were recorded with an Axopatch 200A amplifier (Axon Instruments) and stored on line on a pentium (90 MHz) computer, via a Digidata 1200 interface (Axon Instruments). Data were sampled every 100 μs, or every 20 μs in tail current experiments, and filtered online at 1–2 kHz. All voltages were corrected offline for liquid junction potential (Neher, 1995), measured to be −15 mV in these solutions. The holding potential was between −90 and −115 mV unless otherwise noted (in steady-state inactivation experiments), and voltage steps to different depolarizing potentials with different durations were delivered using pClamp6 software (Axon Instruments). Every patch was examined with 10 ramps (300 ms) from −115 (or −90) to 65 mV, followed by

at least 10 episodes (100–400 ms long) at each depolarizing voltage step between −35 and 5 mV, in 5 or 10 mV intervals.

Leak subtraction was performed by averaging segments of traces with no activity from the same voltage protocol in the same experiment, and subtracting this average from each episode using pClamp6. Single channels were analyzed with pClamp6, and usually no extra filtering was added, but in long episodes (i.e., 400 ms) the data were further Gaussian filtered at 500–1000 Hz. Single channel amplitudes were measured by the pClamp6 software, setting a threshold of 50%, manually examining each opening, and accepting the measured amplitude only of fully resolved openings (>1 ms). Mean open channel amplitudes were determined from amplitude histograms of these single open events. I–V relationships were obtained by plotting the mean current amplitudes determined from each experiment. For calculation of single channel conductances, a linear regression was performed to all points of the I–V relationship below 0 mV for the small channels and below 5 mV for the large channels. For the small conductance channels, openings to an apparent subconductance level were occasionally observed and are seen in the all-points histogram in Figure 2d. These have not been examined further in the present study.

Acknowledgments

This work was supported by Wellcome Trust. A. M. was also partially supported by a British Council–Clore Foundation Award and an Israeli Academy of Science and Humanities–Royal Society grant. We are grateful to Dr. N. S. Berrow and Dr. K. M. Page for the development of this expression system and, together with I. Tedder and D. Bell, for subcloning the cDNAs. We thank Dr. C. N. Wyatt for the NG108–15 cells and Ms. M. Li for COS7 cell culture and transfection. We are grateful to Dr. T. Snutch, Dr. Y. Mori, Dr. H. Chin, Dr. E. Perez-Reyes, Dr. S. Moss, and Dr. T. Hughes for gifts of cDNAs; and to Dr. A. Mathie, Dr. G. Moss, and Dr. T. J. A. Allen for fruitful discussion of the manuscript.

Received November 11, 1997; revised December 22, 1997.

References

Akaike, N., Kostyuk, P.G., and Osipchuk, Y.V. (1989). Dihydropyridine-sensitive low-threshold calcium channels in isolated rat hypothalamic neurones. J. Physiol. (Lond.) *412*, 181–195.

Armstrong, C.M., and Matteson, D.R. (1985). Two distinct populations of calcium channels in a clonal line of pituitary cells. Science *227*, 65–67.

Barish, M.E. (1991). Voltage-gated calcium currents in cultured embryonic *Xenopus* spinal neurones. J. Physiol. (Lond.) *444*, 523–543.

Beam, K.G., and Knudson, C.M. (1988). Calcium currents in embryonic and neonatal mammalian skeletal muscle. J. Gen. Physiol. *91*, 781–798.

Bean, B.P. (1985). Two kinds of calcium channels in canine atrial cells. J. Gen. Physiol. *86*, 1–30.

Berjukow, S., Doring, S., Froschmayr, M., Grabner, M., Glossmann, H., and Hering, S. (1996). Endogenous calcium channels in human embryonic kidney (HEK293) cells. Br. J. Pharmacol. *118*, 748–754.

Berrow, N.S., Brice, N.L., Tedder, I., Page, K., and Dolphin, A.C. (1997). Properties of cloned rat α_{1A} calcium channels transiently expressed in the COS7 cell line. European J. Neurosci. *9*, 739–748.

Bourinet, E., Zamponi, G.W., Stea, A., Soong, T.W., Lewis, B.A., Jones, L.P., Yue, D.T., and Snutch, T.P. (1996). The α_{1E} calcium channel exhibits permeation properties similar to low voltage–activated calcium channels. J. Neurosci. *16*, 4983–4993.

Brice, N.L., Berrow, N.S., Campbell, V., Page, K.M., Brickley, K., Tedder, I., and Dolphin, A.C. (1997). Importance of the different β subunits in the membrane expression of the α_{1A} and α2 calcium channel subunits: studies using a depolarization-sensitive α_{1A} antibody. Eur. J. Neurosci. *9*, 749–759.

Brust, P.F., Simerson, S., McCue, A.F., Deal, C.R., Schoonmaker, S., Williams, M.E., Veliçelebi, G., Johnson, E.C., Harpold, M.M., and Ellis, S.B. (1993). Human neuronal voltage-dependent calcium channels: studies on subunit structure and role in channel assembly. Neuropharmacology *32*, 1089–1102.

Campbell, V., Berrow, N., Brickley, K., Page, K., Wade, R., and Dolphin, A.C. (1995). Voltage-dependent calcium channel β-subunits in combination with α_1 subunits have a GTPase activating effect to promote hydrolysis of GTP by G α_o in rat frontal cortex. FEBS Lett. *370*, 135–140.

Carbone, E., and Lux, H.D. (1984). A low voltage–activated fully inactivating Ca channel in vertebrate sensory neurones. Nature *310*, 501–502.

Carbone, E., and Lux, H.D. (1987a). Single low voltage–activated calcium channels in chick and rat sensory neurones. J. Physiol. (Lond.) *386*, 571–601.

Carbone, E., and Lux, H.D. (1987b). Kinetics and selectivity of a low voltage–activated calcium current in chick and rat sensory neurones. J. Physiol. (Lond.) *386*, 547–570.

Castellano, A., Wei, X., Birnbaumer, L., and Perez-Reyes, E. (1993). Cloning and expression of a third calcium channel β subunit. J. Biol. Chem. *268*, 3450–3455.

Chen, C., and Hess, P. (1990). Mechanism of gating of T-type calcium channels. J. Gen. Physiol. *96*, 603–630.

De Waard, M., and Campbell, K.P. (1995). Subunit regulation of the neuronal α_{1A} Ca^{2+} channel expressed in *Xenopus* oocytes. J. Physiol. (Lond.) *485*, 619–634.

De Waard, M., Witcher, D.R., Pragnell, M., Liu, H., and Campbell, K.P. (1995). Properties of the α_1-β anchoring site in voltage-dependent Ca^{2+} channels. J. Biol. Chem. *270*, 12056–12064.

Dolphin, A.C. (1996). Facilitation of Ca^{2+} current in excitable cells. Trends Neurosci. *19*, 35–43.

Droogmans, G., and Nilius, B. (1989). Kinetic properties of the cardiac T-type calcium channel in the guinea-pig. J. Physiol. (Lond.) *419*, 627–650.

Elmslie, K.S. (1997). Identification of the single channels that underlie the N-type and L-type calcium currents in bullfrog sympathetic neurons. J. Neurosci. *17*, 2658–2668.

Ertel, S.I., and Ertel, E. (1997). Low-voltage-activated T-type calcium channels. Trends Pharmacol. Sci. *18*, 37–42.

Fox, A.P., Nowycky, M.C., and Tsien, R.W. (1987a). Single channel recordings of three types of calcium channels in chick sensory neurones. J. Physiol. (Lond.) *394*, 173–200.

Fox, A.P., Nowycky, M.C., and Tsien, R.W. (1987b). Kinetic and pharmacological properties distinguishing three types of calcium currents in chick sensory neurones. J. Physiol. (Lond.) *394*, 149–172.

Fujita, Y., Mynlieff, M., Dirksen, R.T., Kim, M.-S., Niidome, T., Nakai, J., Friedrich, T., Iwabe, N., Miyata, T., Furuichi, T., et al. (1993). Primary structure and functional expression of the ω-conotoxin-sensitive N-type calcium channel from rabbit brain. Neuron *10*, 585–598.

Gurnett, C.A., Felix, R., and Campbell, K.P. (1997). Extracellular interaction of the voltage-dependent Ca^{2+} channel $\alpha_2\delta$ and α_1 subunits. J. Biol. Chem. *272*, 18508–18512.

Huguenard, J.R. (1996). Low-threshold calcium currents in central nervous system neurons. Annu. Rev. Physiol. *58*, 329–348.

Huguenard, J.R., and Prince, D.A. (1992). A novel T-type current underlies prolonged Ca^{2+}-dependent burst firing in GABAergic neurons of rat thalamic reticular nucleus. J. Neurosci. *12*, 3804–3817.

Hymel, L., Striessnig, J., Glossmann, H., and Schindler, H. (1988). Purified skeletal muscle 1,4-dihydropyridine receptor forms phosphorylation-dependent oligomeric calcium channels in planar bilayers. Proc. Natl. Acad. Sci. USA *85*, 4290–4294.

Kim, H.-L., Kim, H., Lee, P., King, R.G., and Chin, H. (1992). Rat brain expresses an alternatively spliced form of the dihydropyridine-sensitive L-type calcium channel α2 subunit. Proc. Natl. Acad. Sci. USA *89*, 3251–3255.

Kobrinsky, E.M., Pearson, H.A., and Dolphin, A.C. (1994). Low- and high-voltage-activated calcium channel currents and their modulation in the dorsal root ganglion cell line ND7–23. Neuroscience *58*, 539–552.

Lambert, R.C., Maulet, Y., Mouton, J., Beattie, R., Volsen, S., De Waard, M., and Feltz, A. (1997). T-type Ca^{2+} current properties are not modified by Ca^{2+} channel β subunit depletion in nodosus ganglion neurons. J. Neurosci. *17*, 6621–6628.

Liu, J., Rutledge, A., and Triggle, D.J. (1995). Short-term regulation of neuronal calcium channels by depolarization. Ann. N Y Acad. Sci. *765*, 119–133.

McCleskey, E.W., Fox, A.P., Feldman, D.H., Cruz, L.J., Olivera, B.M., Tsien, R.W., and Yoshickami, D. (1987). Omega-conotoxin: direct and persistent blockade of specific types of calcium channels in neurons but not muscle. Proc. Natl. Acad. Sci. USA *84*, 4327–4331.

Neher, E. (1995). Voltage offsets in patch-clamp experiments. In Single Channel Recording, B. Sakmann, and E. Neher, eds. (New York: Plenum Press), pp.147–153.

Nilius, B., Hess, P., Lansman, J.B., and Tsien, R.W. (1985). A novel type of cardiac calcium channel in ventricular cells. Nature *316*, 443–446.

Olcese, R., Qin, N., Schneider, T., Neely, A., Wei, X., Stefani, E., and Birnbaumer, L. (1994). The amino terminus of a calcium channel β subunit sets rates of channel inactivation independently of the subunit's effect on activation. Neuron *13*, 1433–1438.

Olcese, R., Neely, A., Qin, N., Wei, X.Y., Birnbaumer, L., and Stefani, E. (1996). Coupling between charge movement and pore opening in vertebrate neuronal α_{1E} calcium channels. J. Physiol. (Lond.) *497*, 675–686.

Page, K.M., Stephens, G.J., Berrow, N.S., and Dolphin, A.C. (1997). The intracellular loop between domains I and II of the B type calcium channel confers aspects of G protein sensitivity to the E type calcium channel. J. Neurosci. *17*, 1330–1338.

Perez-Reyes, E., Castellano, A., Kim, H.S., Bertrand, P., Baggstrom, E., Lacerda, A.E., Wei, X., and Birnbaumer, L. (1992). Cloning and expression of a cardiac/brain β subunit of the L-type calcium channel. J. Biol. Chem. *267*, 1792–1797.

Schneider, T., Wei, X., Olcese, R., Costantin, J.L., Neely, A., Palade, P., Perez-Reyes, E., Qin, N., Zhou, J., Crawford, G.D., et al. (1994). Molecular analysis and functional expression of the human type E neuronal Ca^{2+} channel α_1 subunit. Receptors Channels *2*, 255–270.

Singer-Lahat, D., Lotan, I., Itagaki, K., Schwartz, A., and Dascal, N. (1992). Evidence for the existence of RNA of Ca^{2+}-channel α_2/δ subunit in *Xenopus* oocytes. Biochim. Biophys. Acta *1137*, 39–44.

Soong, T.W., Stea, A., Hodson, C.D., Dubel, S.J., Vincent, S.R., and Snutch, T.P. (1993). Structure and functional expression of a member of the low voltage-activated calcium channel family. Science *260*, 1133–1136.

Stephens, G.J., Page, K.M., Burley, J.R., Berrow, N.S., and Dolphin, A.C. (1997). Functional expression of rat brain cloned α_{1E} calcium channels in COS7 cells. Pflügers Arch. *433*, 523–532.

Tarasenko, A.N., Kostyuk, P.G., Eremin, A.V., and Isaev, D.S. (1997). Two types of low voltage–activated Ca^{2+} channels in neurones of rat laterodorsal thalamic nucleus. J. Physiol. (Lond.) *499*, 77–86.

Tareilus, E., Roux, M., Qin, N., Olcese, R., Zhou, J.M., Stefani, E., and Birnbaumer, L. (1997). A *Xenopus* oocyte β subunit: evidence for a role in the assembly/expression of voltage-gated calcium channels that is separate from its role as a regulatory subunit. Proc. Natl. Acad. Sci. USA *94*, 1703–1708.

Tomlinson, W.J., Stea, A., Bourinet, E., Charnet, P., Nargeot, J., and Snutch, T.P. (1993). Functional properties of a neuronal class C L-type calcium channel. Neuropharmacology *32*, 1117–1126.

Tsien, R.W., Lipscombe, D., Madison, D., Bley, K., and Fox, A. (1995). Reflections on Ca^{2+}-channel diversity, 1988–1994. Trends Neurosci. *18*, 52–54.

Wakamori, M., Niidome, T., Furutama, D., Furuichi, T., Mikoshiba, K., Fujita, Y., Tanaka, I., Katayama, K., Yatani, A., Schwartz, A., et al. (1994). Distinctive functional properties of the neuronal BII (class E) calcium channel. Receptors Channels *2*, 303–314.

Williams, M.E., Brust, P.F., Feldman, D.H., Patthi, S., Simerson, S., Maroufi, A., McCue, A.F., Veliçelebi, G., Ellis, S.B., and Harpold, M.M. (1992). Structure and functional expression of an omega-conotoxin-sensitive human N-type calcium channel. Science *257*, 389–395.